

## Hexagonal boron-nitride nanomesh magnets

C. Ohata, R. Tagami, Y. Nakanishi, R. Iwaki, K. Nomura, and J. Haruyama

Citation: *Applied Physics Letters* **109**, 133110 (2016); doi: 10.1063/1.4963821

View online: <http://dx.doi.org/10.1063/1.4963821>

View Table of Contents: <http://scitation.aip.org/content/aip/journal/apl/109/13?ver=pdfcov>

Published by the [AIP Publishing](#)

---

### Articles you may be interested in

[Strain tunable electronic and magnetic properties of pristine and semihydrogenated hexagonal boron phosphide](#)  
*Appl. Phys. Lett.* **106**, 043107 (2015); 10.1063/1.4906998

[Intrinsic ferromagnetism in hexagonal boron nitride nanosheets](#)  
*J. Chem. Phys.* **140**, 204701 (2014); 10.1063/1.4879055

[Tunable magnetic states in hexagonal boron nitride sheets](#)  
*Appl. Phys. Lett.* **101**, 132405 (2012); 10.1063/1.4754143

[Magnetic states and optical properties of single-layer carbon-doped hexagonal boron nitride](#)  
*Appl. Phys. Lett.* **100**, 253115 (2012); 10.1063/1.4730392

[Charge-injection induced magnetism and half metallicity in single-layer hexagonal group III/V \(BN, BP, AlN, AlP\) systems](#)  
*Appl. Phys. Lett.* **97**, 093109 (2010); 10.1063/1.3484957

---

The advertisement for Goodfellow features a collage of various materials and components. On the left, there is a list of material types: Pure Metals, Ceramics, Alloys, and Polymers, followed by the text 'in dozens of forms'. The Goodfellow logo is prominently displayed in the center. At the bottom, a blue banner contains the text 'Small quantities fast • Expert technical assistance • 5% discount on online orders'. The background collage includes images of red and white pills, a blue tray with small metal parts, a perforated metal sheet, a yellow metal plate, and a pile of dark powder.

**Pure Metals • Ceramics**  
**Alloys • Polymers**  
in dozens of forms

**Goodfellow**

Small quantities fast • Expert technical assistance • 5% discount on online orders

## Hexagonal boron-nitride nanomesh magnets

C. Ohata, R. Tagami, Y. Nakanishi, R. Iwaki, K. Nomura, and J. Haruyama

*Faculty of Science and Engineering, Aoyama Gakuin University, 5-10-1 Fuchinobe, Sagami-hara, Kanagawa 252-5258, Japan*

(Received 16 June 2016; accepted 19 September 2016; published online 29 September 2016)

The formation of magnetic and spintronic devices using two-dimensional (2D) atom-thin layers has attracted attention. Ferromagnetisms (FMs) arising from zigzag-type atomic structure of edges of 2D atom-thin materials have been experimentally observed in graphene nanoribbons, hydrogen (H)-terminated graphene nanomeshes (NMs), and few-layer oxygen (O)-terminated black phosphorus NMs. Herein, we report room-temperature edge FM in few-layer hexagonal boron-nitride (hBN) NMs. O-terminated hBNNMs annealed at 500 °C show the largest FM, while it completely disappears in H-terminated hBNNMs. When hBNNMs are annealed at other temperatures, amplitude of the FM significantly decreases. These are highly in contrast to the case of graphene NMs but similar to the cases of black phosphorus NM and suggest that the hybridization of the O atoms with B(N) dangling bonds of zigzag pore edges, formed at the 500 °C annealing, strongly contribute to this edge FM. Room-temperature FM realizable only by exposing hBNNMs into air opens the way for high-efficiency 2D flexible magnetic and spintronic devices without the use of rare magnetic elements. *Published by AIP Publishing.* [<http://dx.doi.org/10.1063/1.4963821>]

Realizing room-temperature long-range spin ordering in atomically thin materials is a key to create flexible magnetic and spintronic-devices.<sup>1</sup> High electronic density of states (i.e., edge states) originating from flat energy band of zigzag-type atomic structure of graphene nanoribbon (GNR) edges and subsequently the appearance of flat-band ferromagnetism (FM) were theoretically predicted since old time. They have been recently confirmed experimentally<sup>2–11</sup> in H-terminated zigzag-edged GNRs<sup>3</sup> and also our H-terminated graphene nanomeshes (H-GNMs),<sup>5–9</sup> consisting of a honeycomb-like array of hexagonal nano-pores fabricated using a non-lithographic method which enables formation of the low-disordered and low-contaminated pore edges. Because a GNM corresponds to a large ensemble of GNRs<sup>4</sup> (i.e., inter-pore narrow regions), it is very effective to detect small magnetic signals arising from the pore edge spins.

On the other hand, mono (few)-layer black phosphorus (BP) have been recently found as 2D atom-thin semiconductors.<sup>12–16,21</sup> We clarified that O-terminated zigzag pore edges in few-layer BPNMs produce evident FM with magnitude  $\sim 100$  times/area larger than that reported for the H-GNMs at room temperature.<sup>16</sup> These behaviors highly contrasted with those of H-GNMs as mentioned above. The edge FM was attributed to ferromagnetic spin coupling of the edge P=O bonds and the interlayer ferromagnetic spin coupling due to AB stacking. We clarified those that contribute to it.

These FM promise application to magnetic and spintronic devices realizable without using rare (earth) magnetic elements. Therefore, it is crucial to investigate edge magnetisms in other 2D layers. Here, hexagonal boron-nitride (hBN) is one-atom-thick insulator (e.g., with a wide band gap of 5.92 eV) composed of a hexagonal network with an equal number of alternating B and N atoms in  $sp^2$  hybridization that are bonded covalently. In particular, it has been frequently used to isolate 2D atomic layers from SiO<sub>2</sub> substrate (e.g., rippling and impurities), allowing emergence of high

electron mobility in the 2D layers. On the other hand, edge magnetisms of hBN have been theoretically predicted in hBNNRs and BN anti-dots similar to our nanomesh (NM) structure.<sup>17–20</sup> Reference 17 predicted that H-terminated zigzag BNNRs are non-magnetic, while O-terminated zigzag BNNRs are stable and have two energetically degenerate magnetic ground states with a total magnetic moment of 0.24 and 0.61  $\mu_B$ , respectively. It was reported that the  $p_x$  and  $p_z$  orbitals arising from the edge O-N bond crosses over Fermi level and those spin splitting (particularly, the large spin splitting in the  $p_x$ ) yields the edge FM Half-metallicity realizable by applying electrical fields, was also predicted.

In this work, flakes of few-layer hBNs have been mechanically exfoliated from bulk hBN (Smart Element Co.) in glove box using the Scotch tape method and confirmed using scanning electron microscope (SEM) (Fig. 1(a)) and the observation of Raman spectrum (Fig. 1(b)). Following the non-lithographic method used to engineer GNMs and BPNMs (i.e., using nanoporous alumina template as an etching mask<sup>5–9,16</sup>), few-layer hBNNM have been fabricated and field-emission SEM (FESEM) (Fig. 1(c)) and atomic-force microscope (Figs. 1(d) and 1(e)). Inter-pore narrow regions (e.g., 10–20 nm width) correspond to hBNNRs reported in Ref. 17.

After the formation of nanopore array, the hBNNMs have been annealed at 500 °C, which can be a critical temperature ( $T_c$ ) to form zigzag pore edges through edge atomic reconstruction and produce maximum FM following our previous experiments (as discussed later), and other several temperatures (e.g., 200 °C, 300 °C, 600 °C) in a high vacuum ( $\sim 10^{-6}$  Torr). Presence of either B or N atoms at the edge dangling bonds of the zigzag pores could not be controlled. For O-termination of the pore edges, each hBNNM has been placed in air atmosphere at 300 K for 2–4 h after the  $T_c$  annealing. In contrast, for H-termination, each hBNNM has been annealed in H<sub>2</sub> atmosphere at  $T_c$  for 1 h right after the  $T_c$  annealing. Immediately following this annealing process,

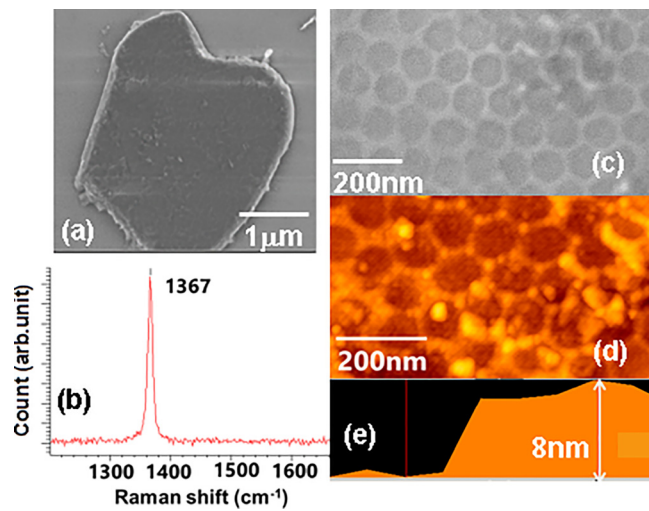


FIG. 1. (a) SEM image of a flake of few-layer hBN mechanically exfoliated from bulk hBN (Smart Element Co.) using the Scotch tape method. (b) Observation of Raman spectrum of (a). (c)–(e) FESEM (c) and AFM ((d) and (e)) images of a few-layer hBNNM fabricated following the non-lithographic method using nano-porous alumina template as an etching mask. Thickness of the hBNNM is  $\sim 8$  nm (e), and pore diameter and inter-pore distance, corresponding to the width of hBN nanoribbons (hBNNRs), are  $\sim 80$  nm and  $\sim 20$  nm ((c) and (d)), respectively.

magnetization has been measured using superconducting quantum interference devices (SQUID: Quantum Design Co.).

The absence of any substantial background magnetic impurities and magnetic contamination (e.g., Ni, Fe, Co) has been carefully confirmed following the previous methods reported in Ref. 16; i.e., (1) the XPS measurements, (2) Confirmation of no magnetic hysteresis loops in few-layer bulk flakes produced using the same fabrication processes as for NM without pore formation, and that in which Ar gas etching process was carried out without using a porous alumina template mask as in the case of NM. (3) Significant differences between magnetization curves for H- and O-hBNNMs discard the introduction of magnetic impurities introduced during the fabrication process. (4) The careful

fabrication process (i.e., bulk hBNs mechanically exfoliated by non-magnetic scotch tapes, porous alumina templates fabricated using extremely pure Al substrate (99.99%) for anodic oxidation, the etching process of hBNs for pore formation using Ar gas, and use of only plastic tweezers during all the fabrication processes).

Figure 2(a) shows a typical measurement result of the magnetization of the few-layer O-hBNNM annealed at  $500^\circ\text{C}$ . Ferromagnetic (FMC)-hysteresis loops are clearly observed within order  $\sim 10^{-4}$  emu, which is almost similar to the magnitude of FM of the few-layer O-BPNMs<sup>16</sup> and larger than that of the H-GNNMs.<sup>5,6</sup> This suggests that spin alignment of the edge O atom is strongly associated with the observed FM. The hysteresis loop at  $T = 2$  K approximately remains unchanged even when increasing the temperature up to  $T = 300$  K. Because few-layer bulk hBN flakes without pores do not exhibit any FMs, this suggests that the FM originates solely from the formation of O-terminated nano-pore edges. The appearance of FM in the O-terminated pore edge is qualitatively consistent with the theory for the zigzag O-hBNNR.<sup>17</sup> Because the inter-pore narrow region of the present hBNNM corresponds to this O-hBNNR, this suggests a possibility that the pore edge atomic structure annealed at  $500^\circ\text{C}$  can be zigzag. This FM has been confirmed at least over five samples. Since the oxidation of pore edges is easily obtained by exposing hBNNMs to air atmosphere, one can assume that all pore edges in an hBNNM are fully O-terminated and can provide a large-magnitude FM. Figure 2(b) shows a temperature dependence of magnetization of Fig. 2(a)-sample at  $H = 10$  Oe. Magnetization monotonically decreases with increasing temperature up to 300 K, which is the upper limit temperature of our SQUID. Hence, Currie temperature of this sample is estimated to be at least above 300 K. It is also interesting to notice that the magnetization value slightly increases below  $\sim 10$  K with decreasing temperature.

On the other hand, Fig. 2(c) with the same field ( $H$ ) range (i.e., x-axis range) as that of Fig. 2(a) shows a measurement result of the magnetization of the few-layer O-hBNNM

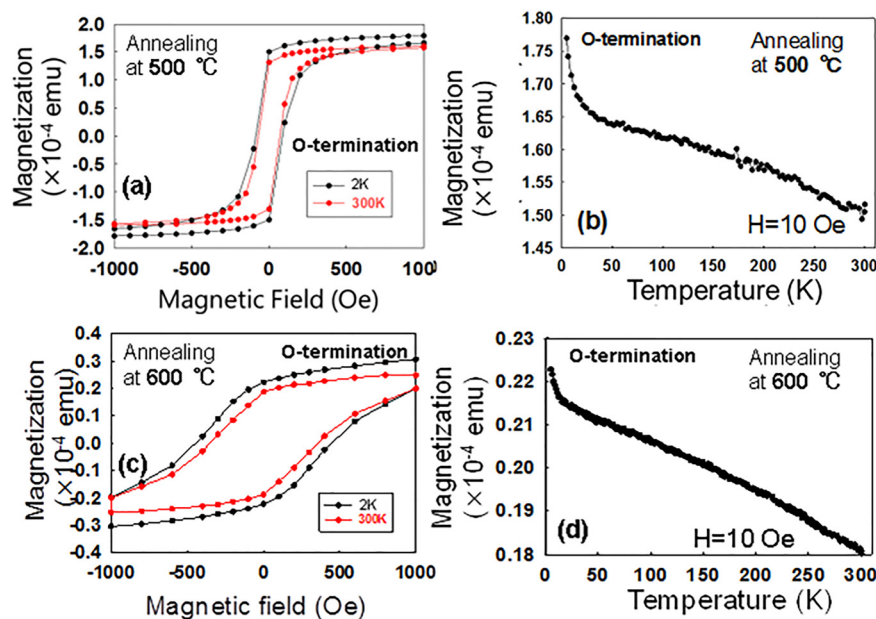


FIG. 2. ((a) and (c)) Typical measurement results of the magnetization curves of the few-layer O-hBNNMs annealed at  $500^\circ\text{C}$  (a) and  $600^\circ\text{C}$  in high vacuum. (c) Sample area is  $\sim 1$  mm<sup>2</sup>. ((b) and (d)) Temperature dependence of (a) and (c), respectively, measured at  $H = 10$  Oe.

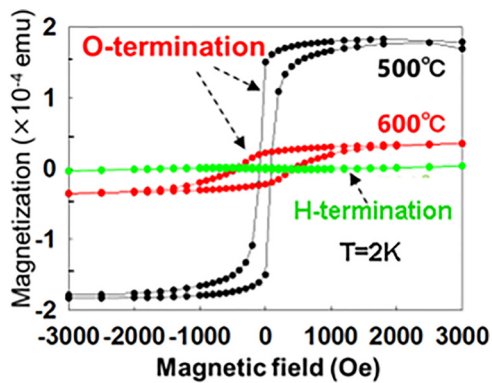


FIG. 3. Magnetization curves of the few-layer O-hBNNMs shown in Figs. 2(a) and 2(c) for the larger  $H$  regime and annealed at 500°C in  $H_2$  atmosphere.

annealed at 600°C. Amplitude of the magnetic hysteresis loop drastically decreases. Residual magnetization decreases almost below one order compared with that of Fig. 2(a). This suggests that the annealing temperature of 600°C cannot be  $T_c$  for the formation of zigzag pore edges. Temperature dependence of Fig. 2(c)-sample is shown in Fig. 2(d). Although the magnetization values are almost one-order smaller than Fig. 2(b), it monotonically decreases with increasing temperature up to 300 K as well as the case in Fig. 2(b). The slight magnetization increase is also observed below  $\sim 10$  K as well as Fig. 2(b).

Figure 3 shows the magnetization curves of the few-layer O-hBNNMs shown in Figs. 2(a) and 2(c) for the larger  $H$  regime and annealed at 500°C in  $H_2$  atmosphere. The difference is much evident. Magnetization value has the largest value in the O-hBNNM annealed at 500°C. For all the samples annealed at temperatures  $> 500$ °C, magnitude of the hysteresis loops drastically decreases and almost disappears like the samples annealed at 600°C. For the hBNNM annealed at 500°C in  $H_2$  atmosphere in Fig. 3, FMC hysteresis loop disappears completely.

Figure 4 shows magnetization curves of the few-layer O-hBNNM annealed at 200°C and 300°C. Although FMC hysteresis loops still remain, the FM amplitudes decrease one order compared to Fig. 2(a) as well as the case for Fig. 2(c) (or Fig. 3), while diamagnetism component appears in the background of the FM as magnetic field increases in contradiction to the case of Fig. 2(c).

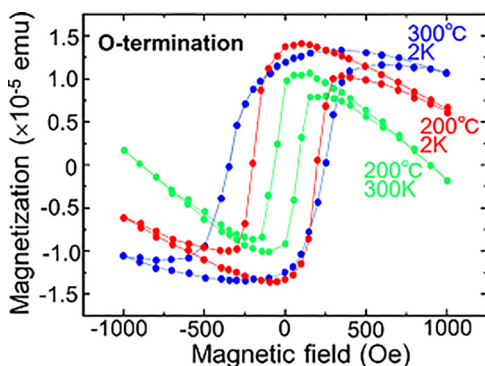


FIG. 4. Magnetization curves of the few-layer O-hBNNMs annealed at 200°C and 300°C in high vacuum.

We discuss correlation of the observed dependence of the magnetism on annealing temperatures with the formation of the zigzag pore edges, based on our previous results, which revealed  $T_c$  of 700°C and 300°C in GNMs and BPNMs, respectively, at which magnetization exhibited the largest FM values. These FM values were attributed to the formation of the zigzag-atomic type pore edges, which were confirmed by Raman spectrum and magnetic force microscope,<sup>5,6,16</sup> by the  $T_c$  annealing through the edge atomic reconstruction. There are some theories and calculations for the formation of zigzag edges. Basically, there are two edge atomic structures, i.e., zigzag with each one dangling bond and arm chair with each two dangling bonds. One theory suggests that the presence of one dangling bond at edges is thermally and chemically stable compared to the case of two dangling bonds, when edge atomic reconstruction occurs. After the removal of edge atoms at the reconstruction, the armchair edge requires energy two times larger than zigzag in order to repair the removed atoms and, thus, becomes unstable. This theory was supported by Refs. 10 and 11, in which STM Joule heating<sup>10</sup> or electron beam irradiation<sup>11</sup> at critical energies produced pure and fully zigzag edge in graphene edges, and corresponded to the  $T_c$  annealing. This process for the zigzag edge formation should be qualitatively the same through C, P, and hBN atoms, when the  $T_c$  annealing yields the maximum FM, although C atom forms pure honeycomb lattice, P atom forms puckered honeycomb lattice, and hBN consists of honeycomb lattice with two different kinds of atoms (B and N). Indeed, Ref. 22 reported observation of the edge atomic structure of a hole fabricated on hBN by scanning transmission electron microscope (STEM) and turned out that zigzag structure is formed at the hole edge with stability sufficient for prolonged observation (at least over a few minutes). This is similar to the case of Ref. 11. Therefore, the annealing at  $T_c = 500$ °C, which introduced the largest FM, can be assumed to create the zigzag pore edge also in the present hBNNM.

For the hBNNM annealed at 500°C in  $H_2$  atmosphere in Fig. 3, FM disappeared. This also agrees with a theory,<sup>17</sup> which predicted the non-magnetic state of zigzag H-hBNNRs, and supports that the zigzag pore edges have been formed and H-terminated by the  $T_c$  annealing. These results are highly in contradiction to the case of GNMs (i.e., zigzag H-GNMs showed flat-band FM, while it disappeared in O-GNMs with diamagnetism) but similar to the case for BPNMs (i.e., O-BPNMs exhibited FM arising from the edge P=O bonds, but it disappeared in H-BPNMs).

On the other hand, the following two differences are unique to hBNNMs, compared to the cases of GNMs and BPNMs. (1) In the cases of GNMs and BPNMs, the samples completely disappeared in AFM and FESEM observation when they were annealed at temperature even 10°C higher than the  $T_c$ , because the inter-pore narrow regions are NRs (10–20 nm width) and easily eliminated via the edge atomic reconstruction and thermal diffusion of C(P) atoms. This also suggested that the  $T_c$  had actually critical energy for the edge reconstruction of the NR structure. In contrast, the present hBPNMs still remained even after the annealing at 600°C ( $\gg T_c = 500$ °C), although the magnetization amplitude drastically decreased. This means a possibility that the

hBNNM structure (i.e., interpore hBNNR regions) is gradually destroyed above  $T_c = 500^\circ\text{C}$  due to the different strength in chemical bonds consisting of two different atoms (i.e., B and N atoms). (2) The annealing at the temperatures  $\ll T_c$  (Fig. 4) led to appearance of the background diamagnetism. This can be attributed to the formation of partial zigzag pore edges mixed with arm chair or chiral edges due to low-energy reconstruction, because Refs. 10 and 11 reported that the annealing with energies lower than the critical energies resulted in arm chair or chiral edges. In this sense, the observed background diamagnetism may be associated with O-arm chair pore edges.

Electronic structures and magnetic behaviors of the present O-hBNNMs can be qualitatively understood based on Ref. 17 as follows. The valence electronic structure of zigzag H-hBNNRs (i.e., with H-B edge dangling bonds on one side of a zigzag NR and H-N bonds on the other side) consists of four groups of twenty bands and a single band crossing the uppermost group. Because any bands locate far from Fermi level ( $E_F$ ) (Fig. 5(a)), it actually shows no FM. This agrees with the result of Fig. 3.

On the other hand, in the spin-resolved component of FMC O-hBNNR compared with this band structure, the main differences arose from the four bands existing around the  $E_F$ , which can be based on the hybridization of the edge O atoms. Each edge O atom undertakes a  $sp$  hybridization yielding two hybrid orbitals along the  $y$  direction. One  $sp$  orbital points toward the B (N) atom forming an O-B (O-N)  $\sigma$ -bond, whereas the other  $sp$  orbital is a lone pair pointing outward. The other two mutually perpendicular  $p_x$  and  $p_z$  orbitals on each O atom are approximately degenerate and accommodate a total of three electrons. The near degeneracy of  $p_x$  and  $p_z$  can be partly removed by their symmetry-allowed mixings with the  $\sigma$ - or  $\pi$ -bands on the BN network, respectively, which add additional  $\pi$ -bond character to the O-B and O-N bonds. Although this  $p_x$  orbital crosses over  $E_F$  at the edge O-B bond, the very small spin splitting yields less contribution to the observed edge FM (black lines in Fig. 5(b)). On the other side, contrary to both the  $p_x$  and  $p_z$  orbitals at the edge, O-N bond crosses over  $E_F$  and those spin splitting contribute to the observed edge FM (red lines in Figs. 5(b) and 5(c)). In particular, the large spin splitting in

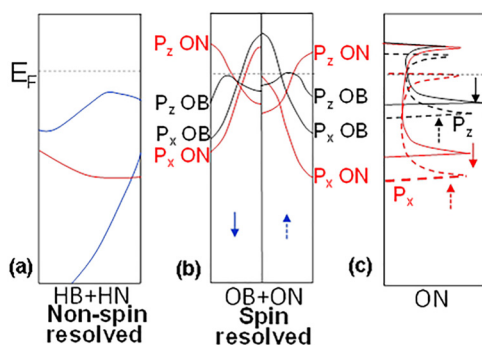


FIG. 5. Schematic image of valence band structures of zigzag hBNNRs reported in Ref. 17. (a) Non-spin resolved valence bands of H-hBNNRs, showing the top and bottom of one typical band (two blue lines) near to  $E_F$  and one band crossing it (red line). (b) Spin-resolved typical four valence bands of O-hBNNRs around  $E_F$  for edge O-B (black lines) and O-N bonds (red lines). (c) Density of spin states for edge O-N bond corresponding to (b).

the  $p_x$  induces the observed edge FM (Fig. 5(c)) as well as the case for the FMC spin coupling in the edge O=P bonds of BPNMs. The slight increase in magnetization values at  $T < \sim 10\text{K}$  observed in Figs. 2(b) and 2(d) may be associated with this spin splitting.

For H-GNMs and O-BPNMs, we have carried our simple estimation of the edge magnetic moment. However, for the present O-hBNNMs, there are two kinds of edge dangling bonds (i.e., O-B or O-N) and we have no data about it. Thus, simple estimation of the magnetization per edge O-B or O-N bond is difficult. Considering this, correlation of the magnetization values with interpore distance and layer number (thickness) is also expected to be clarified.

In conclusion, we have reported the observation of room-temperature edge FM in few-layer O-hBNNMs. O-hBNNMs showed room-temperature FM when annealed at  $500^\circ\text{C}$ , while magnitude of the FM significantly decreased in annealing at other temperatures, suggesting that  $500^\circ\text{C}$  can be the  $T_c$  to form the zigzag pore edges. The FM completely disappeared in H-hBNNMs. These are highly in contrast to the case of H-GNMs, but similar to the cases of O-BPNMs. The large spin splitting in  $p_x$  orbitals caused by hybridization of the O atoms with N dangling bonds of zigzag pore edges strongly contributes to this edge FM, following Ref. 17. Observation of the pore-edge atomic structure (e.g., by high-resolution AFM, TEM<sup>22</sup>), particularly kinds of atoms (B or N) existing at dangling bond, is indispensable. hBNNM has a significant advantage in which O-termination of the edges realizable only by exposing samples into air generate room-temperature magnetism, in contrast to the much smaller FM obtained by partially H-terminated edges in GNMs. It is highly expected that this hBN magnet opens the doors to realize high-efficiency 2D flexible magnetic and spintronic devices without the use of rare magnetic elements.

The authors thank J. Shimoyama, J. Akimitsu, K. Horigane, T. Enoki, Y. Otani, S. Murakami, M. Yamamoto, S. Tarucha, T. Ando, P. Seneor, A. H. Macdonald, R. Wiesendanger, and M. S. Dresselhaus for their technical contributions, fruitful discussions, and encouragements. This work at Aoyama Gakuin was partly supported by a Grant-in-aid for Scientific Research (Basic research A: 24241046 and Challenging Exploratory Research: 15K13277) and grant for private University in MEXT and AOARD grant (135049) in U.S. Air Force Office of Scientific Research.

<sup>1</sup>S. Roche, J. Åkerman, B. Beschoten, J.-C. Charlier, M. Chshiev, S. P. Dash, B. Dlubak, J. Fabian, A. Fert, and M. Guimarães, *2D Mater.* **2**, 030202 (2015).

<sup>2</sup>D. Soriano, N. Leconte, P. Ordejón, J.-C. Charlier, J.-J. Palacios, and S. Roche, *Phys. Rev. Lett.* **107**, 016602 (2011).

<sup>3</sup>G. Z. Magda, X. Jin, I. Hagymási, P. Vancsó, Z. Osváth, P. N.-Incze, C. Hwang, L. P. Biró, and L. Tapasztó, *Nature* **514**, 608 (2014).

<sup>4</sup>T. Shimizu, J. Haruyama, T. Shimizu, J. Haruyama, D. C. Marcano, D. V. Kosinkin, J. M. Tour, K. Hirose, and K. Suenaga, *Nat. Nanotechnol.* **6**, 45 (2011).

<sup>5</sup>J. Haruyama, *Electronics*, Special Issue on “Carbon Nanoelectronics” **2**(4), 368–386 (2013).

<sup>6</sup>K. Tada, J. Haruyama, H. Yang, and M. Chshiev, *Phys. Status Solidi B* **249**, 2491 (2012).

<sup>7</sup>T. Kato, T. Nakamura, and J. Haruyama, *Appl. Phys. Lett.* **104**, 252410 (2014).

- <sup>8</sup>T. Hashimoto, J. Haruyama, D. Soriano, and S. Roche, *Appl. Phys. Lett.* **105**, 183111 (2014).
- <sup>9</sup>T. Hashimoto, S. Kamikawa, Y. Yagi, and J. Haruyama, *Mater. Sci. Appl.* **5**(1), 1 (2014).
- <sup>10</sup>X. Jia, M. Hofmann, V. Meunier, B. G. Sumpter, J. C.-Delgado, J. M. Romo-Herrera, H. Son, Y.-P. Hsieh, A. Reina, J. Kong *et al.*, *Science* **323**, 1701 (2009).
- <sup>11</sup>C. O. Girit, J. C. Meyer, R. Erni, M. D. Rossell, C. Kisielowski, L. Yang, C.-H. Park, M. F. Crommie, M. L. Cohen, S. G. Louie *et al.*, *Science* **323**, 1705 (2009).
- <sup>12</sup>L. Li, Y. Yu, G. J. Ye, Q. Ge, X. Ou, H. Wu, D. Feng, X. H. Chen, and Y. Zhang, *Nat. Nanotechnol.* **9**, 372 (2014).
- <sup>13</sup>H. O. H. Churchill and P.-J. Herrero, *Nat. Nanotechnol.* **9**, 330 (2014).
- <sup>14</sup>A. C.-Gomez, L. Vicarelli, E. Prada, J. O. Island, K. L. N.-Acharya, S. I. Blanter, D. J. Groenendijk, M. Buscema, G. A. Steele, and J. V. Alvarez, *2D Mater.* **1**, 025001 (2014).
- <sup>15</sup>Z. Zhu, C. Li, W. Yu, D. Chang, Q. Sun, and Y. Jia, *Appl. Phys. Lett.* **105**, 113105 (2014).
- <sup>16</sup>T. Nakanishi, R. Iwaki, K. Nomura, C. Ohata, D. Soriano, S. Roche, and J. Haruyama, *Nano Res.*; See <http://www.ee.aoyama.ac.jp/Labs/j-haru-www/>.
- <sup>17</sup>A. L.-Bezanilla, A. L.-Bezanilla, J. Huang, H. Terrones, and B. G. Sumpter, *Nano Lett.* **11**, 3267 (2011).
- <sup>18</sup>A. Du, Y. Chen, Z. Zhu, R. Amal, G. Qing (Max) Lu, and S. C. Smith, *J. Am. Chem. Soc.* **131**, 17354 (2009).
- <sup>19</sup>V. Barone and J. E. Peralta, *Nano Lett.* **8**, 2210 (2008).
- <sup>20</sup>C.-H. Park and S. G. Louie, *Nano Lett.* **8**, 2200 (2008).
- <sup>21</sup>T. Makino, C. Ohata, and J. Haruyama, *Appl. Phys. Lett.*; See <http://www.ee.aoyama.ac.jp/Labs/j-haru-www/>.
- <sup>22</sup>N. Alem, Q. M. Ramasse, C. R. Seabourne, O. V. Yazyev, K. Erickson, M. C. Sarhan, C. Kisielowski, A. J. Scott, S. G. Louie, and A. Zettl, *Phys. Rev. Lett.* **109**, 205502 (2012).